IEEE Access
Multidisciplinary ⋮ Rapid Review ⋮ Open Access Journal

Received June 7, 2022, accepted June 14, 2022, date of publication June 17, 2022, date of current version June 23, 2022.

Digital Object Identifier 10.1109/ACCESS.2022.3184005

Design of a Modal Controller With Simple Models for an Active Suspension System

MANBOK PARK[1], YONGHWAN JEONG[2], AND SEONGJIN YIM[3], (Member, IEEE)

[1]Department of Electronic Engineering, Korea National University of Transportation, Chungju-si, Chungcheongbuk-do 27469, Republic of Korea
[2]Department of Mechanical and Automotive Engineering, Seoul National University of Science and Technology, Nowon-gu, Seoul 01811, Republic of Korea
[3]Research Center for Electrical and Information Technology, Seoul National University of Science and Technology, Nowon-gu, Seoul 01811, Republic of Korea

Corresponding author: Seongjin Yim (acebtif@seoultech.ac.kr)

This research was supported by the National Research Foundation of South Korea (NRF) Grant funded by the Korean Government through the Ministry of Education under Grant 2019R1A6A1A03032119.

ABSTRACT This paper presents a method to design a modal controller with simple 1-DOF models for an active suspension system. Full-state feedback controller, especially, linear quadratic regulator (LQR) and H_∞ controller, designed with 7-DOF full-car model is hard to implement in actual vehicles because there are so many state variables and gain elements needed to be precisely measured and finely tuned, respectively. To overcome the problem, it is required to design a simple controller with a smaller number of gain elements and sensor signals. For the purpose, a modal controller is designed from controllers designed with three 1-DOF models describing heave, roll and pitch motions of a sprung mass. With these 1-DOF models, discrete-time LQR and sliding mode control (SMC) are adopted to design three feedback controllers which generate vertical force, roll and pitch moments for controlling the heave, roll and pitch motions of a sprung mass, respectively. In the modal controller, three control inputs are converted into active forces at four corners with input decoupling transformation. The modal controller is a type of static output feedback (SOF) one. By LQ SOF control methodology, the modal controller itself is designed with a heuristic optimization method. A frequency domain analysis and a simulation on vehicle simulation software, CarMaker®, show that the proposed modal controllers are effective in controlling the active suspension system for ride comfort.

INDEX TERMS Active suspension control, modal control, 1-DOF vehicle model, linear quadratic regulator, sliding mode control, LQ static output feedback control.

NOMENCLATURE

c_s	damping coefficient of suspension of quarter-car model
c_{si}	damping coefficient of suspension of full-car model, $i = 1,2,3,4$
C_z	damping coefficient of 1-DOF heave model
C_ϕ	roll damping coefficient of 1-DOF roll model
C_θ	pitch damping coefficient of 1-DOF pitch model
f_q	suspension force of quarter-car model
f_i	suspension force of full-car model, $i = 1,2,3,4$
f_{zc}	control force of 1-DOF heave model
h_r	height of center of gravity of 1-DOF roll model
h_p	height of center of gravity of 1-DOF pitch model
I_x	roll moment of inertia in full-car model
I_y	pitch moment of inertia in full-car model
J_q	LQ objective function for quarter-car model
J_f, J_{fq}	LQ objective functions for full-car model
J_z, J_ϕ, J_θ	LQ objective functions for 1-DOF heave, roll and pitch models
K_z	spring stiffness of 1-DOF heave model
K_ϕ	roll stiffness of 1-DOF roll model
K_θ	pitch stiffness of 1-DOF pitch model
k_s	spring stiffness of suspension of quarter-car model
k_{si}	spring stiffness of suspension of full-car model, $i = 1,2,3,4$
k_t	tire stiffness of quarter-car model
k_{ti}	tire stiffness of full-car model, $i = 1,2,3,4$
l_f, l_r	distances from center of gravity to front and rear axles
M_ϕ	control roll moment of 1-DOF roll model
M_θ	control pitch moment of 1-DOF pitch model
m_f	sprung mass of full-car model

The associate editor coordinating the review of this manuscript and approving it for publication was Qi Zhou.

m_u	unsprung mass of quarter-car model
m_s	sprung mass of quarter-car model
m_u	unsprung mass of quarter-car model
t_f, t_r	half of track width of front and rear axles
T_s	sampling time or rate in discrete-time model
u_q	control input in quarter-car model
u_i	control input in full-car model, $i = 1,2,3,4$
z_c	vertical displacement of sprung mass in full-car model
z_r	road profile acting on unsprung mass in quarter-car model
z_{ri}	road profile acting on unsprung mass in full-car model, $i = 1,2,3,4$
z_s	vertical displacement of sprung mass of quarter-car model
z_{si}	vertical displacement of sprung mass at each corner in full-car model
z_u	vertical displacement of unsprung mass in quarter-car model
z_{ui}	vertical displacement of unsprung mass in full-car model, $i = 1,2,3,4$
z_v	vertical displacement of 1-DOF heave model
α	tuning parameter for convergence speed in SMC
ϕ	roll angle of sprung mass in full-car model
ϕ_v	roll angle of 1-DOF roll model
η	maximum allowable value of each term in J
θ_v	pitch angle of sprung mass in full-car model
θ	pitch angle of 1-DOF pitch model
ρ	maximum allowable value on each term in J_q, J_f and J_{fq}
ζ_i, ξ_i, σ_i	maximum allowable values on each term in J_z, J_ϕ and J_θ, $i = 1,2,3$

I. INTRODUCTION

Generally, ride comfort and road holding are two key goals for vehicle suspension design. These are directly related to two physical measures: vertical acceleration of a sprung mass and tire deflection, respectively [1]. According to ISO2631-1, ride comfort is evaluated with vertical acceleration of a sprung mass [2], [3]. On the other hand, Road holding depends on tire deflection. It has been well known that there is conflict between the two goals, i.e., ride comfort and road holding [1], [4], [5]. In other words, the one is improved while the other is deteriorated.

An active suspension system has been developed for the purpose of improving ride comfort by reducing the vertical acceleration of a sprung mass with an active actuator. Up to now, lots of studies on controller design methods for an active suspension system have been done [6]–[8]. Since 2015, LQR, LQ SOF control, H_∞ control, fuzzy control, adaptive control, sliding mode control, back-stepping control, neural network based control and model predictive control (MPC) have been adopted as controller design methodology [9]–[22]. Most of these papers have taken actuator limitations and state constraints such as actuator saturation, actuator bandwidth, dynamic tire load and suspension space limits into account in controller design stage. However, no actuator dynamics was considered nor experimental investigation was done in those studies except the reference [12].

Among the controller design methodologies applied to an active suspension system, LQR and H_∞ control have been adopted because those can systematically design a full-state feedback controller [1], [4], [5], [13], [21], [22]. Those controllers have been designed with the 2-DOF quarter-car, 4-DOF half-car and 7-DOF full-car models. Hereafter, the terms 2-DOF and 7-DOF are omitted. Most of studies [9]–[22] have used the quarter-car model except two studies [13], [15] because it is simple to be used for controller design and performance analysis on active suspension system. However, this model cannot handle the roll and pitch motions of a sprung mass. Whereas, the full-car model is most pertinent to controller design for an active suspension system because it can handle the roll and pitch motions of a sprung mass [5]. Meanwhile, a LQR designed with the quarter-car model has not been used for the full-car case except in two studies [21], [22]. In the previous studies, the LQR designed with the quarter-car model was adopted for the full-car model and it was verified that it can provide equivalent performance to LQR designed with the full-car model [21], [22].

The number of state variables in the state-space equation derived from the full-car model is fourteen. Hence, these state variables must be measured if the full-car model is used to design a full-state feedback controller, e.g., LQR and H_∞ controller, for an active suspension system. However, it is difficult to measure the state variables in the model using sensors on actual vehicles. To overcome this problem, a state observer or an output feedback controller such as Kalman filter or LQG has been designed with the model [13], [23]. Moreover, it is also difficult to implement a full-state feedback controller designed with the full-car model on an actual vehicle because the size of gain matrix in the full-state feedback controller is large. For example, there are four control inputs in the full-car model. Hence, the dimension of the gain matrix of the full-state feedback controller is 4×14, which is too large to be implemented in actual vehicles. For this reason, it is challenging to implement the full-state feedback controller on actual vehicles or on vehicle simulation software such as CarMaker or CarSim. Therefore, it is required to design a controller with fewer sensor signals for feedback control and fewer elements in the gain matrix.

For the purpose in this paper, a modal control can be adopted as a controller design methodology [24]–[30]. The first step of the modal control is to design three controllers separately for heave, roll and pitch motions of a sprung mass [24], [30]. Let these controllers denote heave, roll and pitch controllers, respectively. The second step of the modal control is to convert three control inputs calculated from heave, roll and pitch controllers to four ones at each corner with input decoupling transformation [25], [26], [29]. The controllers designed in the first step have a simpler structure and require a smaller number of states for feedback.

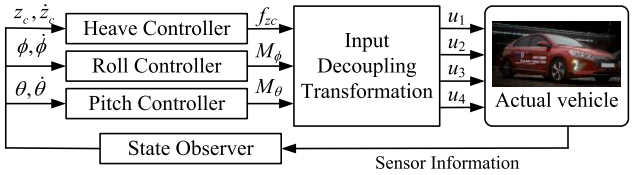

FIGURE 1. Schematic diagram of the modal controller for an active suspension system.

Following the idea of the modal control, this paper uses three 1-DOF simple models describing heave, roll and pitch motions of a sprung mass. Three controllers, i.e., heave, roll and pitch controllers, are designed with corresponding three 1-DOF models using discrete-time LQR and SMC in order to generate vertical force, roll and pitch moments, respectively. Each controller requires two state variables for feedback. So, six state variables are needed for active suspension control. Three control force and moments are converted into four vertical control forces at each corner. Compared to LQR designed with the full-car model, this controller requires six state variables and has six corresponding gain elements. Fig. 1 shows the schematic diagram of the modal controller to be designed in this paper [25], [29]. As shown in Fig. 1, the heave, roll and pitch controllers require two sensor signals, and generate the vertical force and roll and pitch moments. These three control inputs are converted into control forces at four corners with input decoupling transformation.

The modal controller designed in this paper is a type of structured SOF controller [21], [25], [29]. For example, the dimension of the gain matrix of the modal controller adopted in this paper is 3×6, which means that there are six sensor signals and three control inputs. However, there are six non-zero gain elements in the gain matrix. Hence, this is a structured controller, as given in [22], [25], [29]. For this reason, the gain matrix of the modal controller can be determined by LQ SOF control methodology. In this paper, a heuristic optimization method is adopted to find an optimum gain matrix of the modal controller.

The contributions of this paper are condensed as follows:

1) For active suspension control, the modal controller is designed with 1-DOF simple models describing the heave, roll and pitch motions of a sprung mass.
2) Discrete-time LQR and sliding mode control are adopted to design controllers with 1-DOF simple models. Among them, sliding mode control is quite simple to design.
3) The modal controller is designed with LQ SOF control methodology. For the purpose, an optimization problem is formulated and the solution of the problem is obtained by a heuristic optimization method.

To evaluate the performance of the proposed modal controllers for an active suspension system, an analysis on frequency responses and a simulation on the vehicle simulation software, CarMaker, are done. The designed modal controllers are compared with one another using the analysis and simulation from the viewpoint of ride comfort.

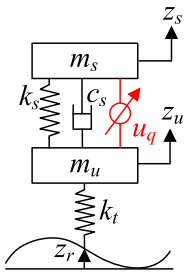

FIGURE 2. 2-DOF quarter-car model.

This paper is organized with four sections. In Section II, discrete-time state-space equations are derived from quarter-car, full-car and three 1-DOF models. With those equations obtained from 1-DOF models, the discrete-time LQR and sliding mode controller are designed. In Section III, for the designed controllers, singular value plots are drawn and simulations on a vehicle simulation software are done. Section IV concludes this paper.

II. CONTROLLER DESIGN FOR ACTIVE SUSPENSION

A. CONTROLLER DESIGN WITH QUARTER-CAR AND FULL-CAR MODELS

Fig. 2 shows a quarter-car model, which describes the vertical motions of the sprung and unsprung masses. The control input u_q is generated by an actuator. The disturbance is the road profile.

The force f_q acting on the sprung and unsprung masses is calculated as (1) with the suspension displacement and its velocity. With f_q, the equations of motion of the quarter-car model are derived as (2). The state vector of the quarter-car model is defined as (3). With the definition and some algebraic manipulations on (2), the continuous-time state-space equation for the quarter-car model is obtained as (4). the system and input matrices, $\mathbf{A}_q$, $\mathbf{B}_{1q}$ and $\mathbf{B}_{2q}$, are given in (5). The procedure of how to obtain these matrices can be found in the previous study [21]. Those matrices are discretized into Φ_q, Γ_q and Ω_q by (6) with the sampling time T_s. After discretization, the discrete-time state-space equation is obtained as (7).

$$f_q(t) = -k_s\{z_s(t) - z_u(t)\} - c_s\{\dot{z}_s(t) - \dot{z}_u(t)\} + u_q(t) \tag{1}$$

$$\begin{cases} m_s\ddot{z}_s(t) = f_q(t) \\ m_u\ddot{z}_u(t) = -f_q(t) - k_t\{z_u(t) - z_r(t)\} \end{cases} \tag{2}$$

$$\mathbf{x}_q(t) = \begin{bmatrix} z_s(t) & z_u(t) & \dot{z}_s(t) & \dot{z}_u(t) \end{bmatrix}^T \tag{3}$$

$$\dot{\mathbf{x}}_q(t) = \mathbf{A}_q\mathbf{x}_q(t) + \mathbf{B}_{1q}z_r(t) + \mathbf{B}_{2q}u_q(t) \tag{4}$$

$$\mathbf{A}_q = \begin{bmatrix} 0 & 0 & 1 & 0 \\ 0 & 0 & 0 & 1 \\ -\dfrac{k_s}{m_s} & \dfrac{k_s}{m_s} & -\dfrac{c_s}{m_s} & \dfrac{c_s}{m_s} \\ \dfrac{k_s}{m_u} & -\dfrac{(k_s+k_t)}{m_u} & \dfrac{c_s}{m_u} & -\dfrac{c_s}{m_u} \end{bmatrix},$$

$$\mathbf{B}_{1q} = \begin{bmatrix} 0 \\ 0 \\ 0 \\ \dfrac{k_t}{m_u} \end{bmatrix}, \quad \mathbf{B}_{2q} = \begin{bmatrix} 0 \\ 0 \\ \dfrac{1}{m_s} \\ -\dfrac{1}{m_u} \end{bmatrix} \tag{5}$$

$$\begin{cases} \mathbf{\Phi}_q \equiv e^{\mathbf{A}_q T_s} \approx \mathbf{I} + \mathbf{A}_q \cdot T_s \\ \mathbf{\Gamma}_q \equiv \left(\displaystyle\int_0^{T_s} \mathbf{\Phi}_q(\tau)\, d\tau \right) \mathbf{B}_{1q} \approx \mathbf{B}_{1q} \cdot T_s \\ \mathbf{\Omega}_q \equiv \left(\displaystyle\int_0^{T_s} \mathbf{\Phi}_q(\tau)\, d\tau \right) \mathbf{B}_{2q} \approx \mathbf{B}_{2q} \cdot T_s \end{cases} \tag{6}$$

$$\mathbf{x}_q(k+1) = \mathbf{\Phi}_q \mathbf{x}_q(k) + \mathbf{\Omega}_q z_r(k) + \mathbf{\Gamma}_q u_q(k) \tag{7}$$

With the state variables and control input of the quarter-car model, LQ objective function for an active suspension system is defined as (8). The weights $1/\rho_i^2$ in (8) are set by Bryson's rule, where ρ_i is the maximum allowable value on the corresponding term [31]. If a particular ρ_i is reduced while maintaining the other weights constant, then the corresponding term will decrease. For the purpose of improving ride comfort, ρ_1 on the vertical acceleration of the sprung mass must be set to a lower value while maintaining the other ρ_i constant. Whereas, for the purpose of enhancing road holding or cornering, ρ_2 and ρ_3 on the suspension displacement and the tire deflection must be set to a higher one, respectively. The LQ objective function, (8), is converted into the vector-matrix form, (9), with the weighting matrices, $\mathbf{Q}_q$, $\mathbf{N}_q$ and $\mathbf{R}_q$. LQR is a full-state feedback controller, as given in (11), which minimizes J_q. The controller gain matrix $\mathbf{K}_q$ is obtained by solving Riccati equation comprising Φ_q, Ω_q, $\mathbf{Q}_q$, $\mathbf{N}_q$ and $\mathbf{R}_q$. As shown in (11), the number of elements in the gain matrix is 4, which is the same as the number of state variables given in (3).

$$J_q = \sum_{k=0}^{\infty} \left\{ \begin{array}{l} \dfrac{1}{\rho_1^2} \ddot{z}_s^2(k) + \dfrac{1}{\rho_2^2} \{z_s(k) - z_u(k)\}^2 \\ + \dfrac{1}{\rho_3^2} z_u^2(k) + \dfrac{1}{\rho_4^2} u_q^2(k) \end{array} \right\} \tag{8}$$

$$J_q = \sum_{k=0}^{\infty} \begin{bmatrix} \mathbf{x}_q(k) \\ u_q(k) \end{bmatrix}^T \begin{bmatrix} \mathbf{Q}_q & \mathbf{N}_q \\ \mathbf{N}_q^T & \mathbf{R}_q \end{bmatrix} \begin{bmatrix} \mathbf{x}_q(k) \\ u_q(k) \end{bmatrix} \tag{9}$$

$$\rho_i = 1/\eta_i^2, \quad i = 1, 2, 3, 4 \tag{10}$$

$$u_q(k) = -\mathbf{K}_q \mathbf{x}_q(k) = -\begin{bmatrix} k_1 & k_2 & k_3 & k_4 \end{bmatrix} \mathbf{x}_q(k) \tag{11}$$

Fig. 3 shows a full-car model, which describes the heave, roll and pitch motions of a sprung mass, and the vertical motions of 4 unsprung masses. In Fig. 3, the four corners, i.e., front left (FL), front right (FR), rear left (RL) and rear right (RR) ones are indexed as ①, ②, ③ and ④ for convenience, respectively. In the model, there are 4 external disturbances, i.e., the road profiles, z_{r1}, z_{r2}, z_{r3} and z_{r4}, on the unsprung mass. The longitudinal and lateral accelerations caused by braking and cornering are not considered in this paper.

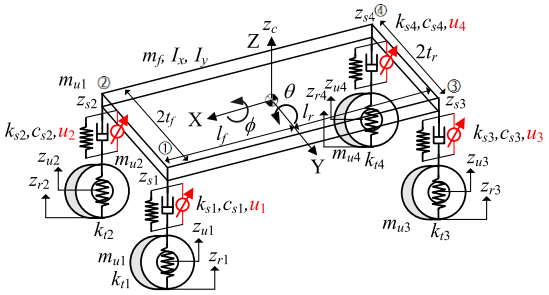

FIGURE 3. 7-DOF full-car model.

The suspension forces at each corner in the model are calculated in (12). In (12), u_i is the control input or active force acting on the i-th suspension or corner. The equations of motion for the sprung and unsprung masses are derived as (13) and (14), respectively. The equations of motion for the sprung mass in (13) can be rewritten into the vector-matrix form of (15). In (15), the matrix $\mathbf{G}$ stands for the geometric relationship between the suspension forces f_i at each corner and the vertical force, roll and pitch moments acting on the sprung mass. This is called input decoupling transformation matrix or modal transform matrix or modal decomposition matrix [24], [25], [30].

$$\begin{aligned} & f_i(t) \\ &= -k_{si}\{z_{si}(t) - z_{ui}(t)\} - c_{si}\{\dot{z}_{si}(t) - \dot{z}_{ui}(t)\} + u_i(t), \\ & \quad i = 1 \cdots 4 \end{aligned} \tag{12}$$

$$\begin{cases} m_f \ddot{z}_c(t) = f_1(t) + f_2(t) + f_3(t) + f_4(t) \\ I_x \ddot{\phi}(t) = t_f \cdot f_1(t) - t_f \cdot f_2(t) + t_r \cdot f_3(t) - t_r \cdot f_4(t) \\ I_y \ddot{\theta}(t) = -l_f \cdot \{f_1(t) + f_2(t)\} + l_r \cdot \{f_3(t) + f_4(t)\} \end{cases} \tag{13}$$

$$m_{ui} \ddot{z}_{ui}(t) = -f_i(t) + k_{ti}\{z_{ui}(t) - z_{ri}(t)\}, \quad i = 1, 2, 3, 4 \tag{14}$$

$$\begin{aligned} & \begin{bmatrix} m_f \ddot{z}_c(t) \\ I_x \ddot{\phi}(t) \\ I_y \ddot{\theta}(t) \end{bmatrix} \\ &= \begin{bmatrix} 1 & 1 & 1 & 1 \\ t_f & -t_f & t_r & -t_r \\ -l_f & -l_f & l_r & l_r \end{bmatrix} \begin{bmatrix} f_1(t) \\ f_2(t) \\ f_3(t) \\ f_4(t) \end{bmatrix} \equiv \mathbf{G} \begin{bmatrix} f_1(t) \\ f_2(t) \\ f_3(t) \\ f_4(t) \end{bmatrix} \end{aligned} \tag{15}$$

To derive the state-space equation, new vectors and matrices are defined in (16) and (17), respectively. With those vectors and geometric relationship of a vehicle, the vertical displacements of four corners are calculated as (18) [21]. With (16), (17) and (18), the suspension forces are converted into the vector-matrix form of (19). The equations of motions of the sprung and unsprung masses are converted into the vector-matrix form of (20). By replacing $\mathbf{f}(t)$ in (20) with (19) and converting (20) into the vector-matrix form, (21) is obtained. With the new definitions of matrices as given in (22), (21) is converted into (23). From the definition of the state vector $\mathbf{x}_f$ and (23), the state-space equation of the full-car model is derived as (24) [21]. The matrices $\mathbf{A}_f$, $\mathbf{B}_{1f}$ and $\mathbf{B}_{2f}$

in (24) are given in (25). By using the formula of (26), the continuous-time state-space equation is discretized into the discrete-time state-space one (27) with the sampling time T_s.

$$\begin{cases} \mathbf{z}_s(t) \triangleq \left[z_{s1}(t) \;\; z_{s2}(t) \;\; z_{s3}(t) \;\; z_{s4}(t) \right]^T \\ \mathbf{z}_u(t) \triangleq \left[z_{u1}(t) \;\; z_{u2}(t) \;\; z_{u3}(t) \;\; z_{u4}(t) \right]^T \\ \mathbf{z}_r(t) \triangleq \left[z_{r1}(t) \;\; z_{r2}(t) \;\; z_{r3}(t) \;\; z_{r4}(t) \right]^T \\ \mathbf{p}(t) \triangleq \left[z_c(t) \;\; \phi(t) \;\; \theta(t) \right]^T \\ \mathbf{q}(t) \triangleq \begin{bmatrix} \mathbf{p}(t) \\ \mathbf{z}_u(t) \end{bmatrix}, \mathbf{x}_f(t) \equiv \begin{bmatrix} \mathbf{q}(t) \\ \dot{\mathbf{q}}(t) \end{bmatrix} \\ \mathbf{w}_f(t) \equiv \left[z_{r1}(t) \;\; z_{r2}(t) \;\; z_{r3}(t) \;\; z_{r4}(t) \right]^T \\ \mathbf{f}(t) \equiv \left[f_1(t) \;\; f_2(t) \;\; f_3(t) \;\; f_4(t) \right]^T \\ \mathbf{u}_f(t) \equiv \left[u_1(t) \;\; u_2(t) \;\; u_3(t) \;\; u_4(t) \right]^T \end{cases} \tag{16}$$

$$\begin{cases} \mathbf{M}_s \triangleq \text{diag}\left(m_s, I_x, I_y\right), \\ \mathbf{M}_u \triangleq \text{diag}\left(m_{u1}, m_{u2}, m_{u3}, m_{u4}\right) \\ \mathbf{K}_s \triangleq \text{diag}\left(k_{s1}, k_{s2}, k_{s3}, k_{s4}\right), \\ \mathbf{K}_t \triangleq \text{diag}\left(k_{t1}, k_{t2}, k_{t3}, k_{t4}\right) \\ \mathbf{C}_s \triangleq \text{diag}\left(c_{s1}, c_{s2}, c_{s3}, c_{s4}\right) \end{cases} \tag{17}$$

$$\mathbf{z}_s(t) = \mathbf{G}^T \mathbf{p}(t) \tag{18}$$

$$\begin{aligned} \mathbf{f}(t) &= -\mathbf{K}_s \left\{ \mathbf{z}_s(t) - \mathbf{z}_u(t) \right\} \\ &\quad - \mathbf{C}_s \left\{ \dot{\mathbf{z}}_s(t) - \dot{\mathbf{z}}_u(t) \right\} + \mathbf{u}_f(t) \\ &= -\mathbf{K}_s \left\{ \mathbf{G}^T \mathbf{p}(t) - \mathbf{z}_u(t) \right\} \\ &\quad - \mathbf{C}_s \left\{ \mathbf{G}^T \dot{\mathbf{p}}(t) - \dot{\mathbf{z}}_u(t) \right\} \\ &\quad + \mathbf{u}_f(t) \end{aligned} \tag{19}$$

$$\begin{cases} \mathbf{M}_s \ddot{\mathbf{p}}(t) = \mathbf{G}\mathbf{f}(t) \\ \mathbf{M}_u \ddot{\mathbf{z}}_u(t) = -\mathbf{f}(t) + \mathbf{K}_t \left\{ \mathbf{z}_u(t) - \mathbf{z}_r(t) \right\} \end{cases} \tag{20}$$

$$\begin{aligned} &\begin{bmatrix} \mathbf{M}_s & \mathbf{0} \\ \mathbf{0} & \mathbf{M}_u \end{bmatrix} \begin{bmatrix} \ddot{\mathbf{p}}(t) \\ \ddot{\mathbf{z}}_u(t) \end{bmatrix} \\ &= \begin{bmatrix} -\mathbf{G}\mathbf{K}_s\mathbf{G}^T & \mathbf{G}\mathbf{K}_s \\ \mathbf{K}_s\mathbf{G}^T & -\mathbf{K}_s + \mathbf{K}_t \end{bmatrix} \begin{bmatrix} \mathbf{p}(t) \\ \mathbf{z}_u(t) \end{bmatrix} \\ &\quad + \begin{bmatrix} -\mathbf{G}\mathbf{C}_s\mathbf{G}^T & \mathbf{G}\mathbf{C}_s \\ \mathbf{C}_s\mathbf{G}^T & -\mathbf{C}_s \end{bmatrix} \begin{bmatrix} \dot{\mathbf{p}}(t) \\ \dot{\mathbf{z}}_u(t) \end{bmatrix} \\ &\quad + \begin{bmatrix} \mathbf{G} \\ -\mathbf{I} \end{bmatrix} \mathbf{u}_f(t) + \begin{bmatrix} \mathbf{0}_{3\times4} \\ -\mathbf{K}_t \end{bmatrix} \mathbf{z}_r(t) \end{aligned} \tag{21}$$

$$\begin{cases} \mathbf{M}_e \triangleq \begin{bmatrix} \mathbf{M}_s & \mathbf{0}_{3\times4} \\ \mathbf{0}_{4\times3} & \mathbf{M}_u \end{bmatrix}, \\ \mathbf{K}_e \triangleq \begin{bmatrix} -\mathbf{G}\mathbf{K}_s\mathbf{G}^T & \mathbf{G}\mathbf{K}_s \\ \mathbf{K}_s\mathbf{G}^T & -\mathbf{K}_s + \mathbf{K}_t \end{bmatrix} \\ \mathbf{C}_e \triangleq \begin{bmatrix} -\mathbf{G}\mathbf{C}_s\mathbf{G}^T & \mathbf{G}\mathbf{C}_s \\ \mathbf{C}_s\mathbf{G}^T & -\mathbf{C}_s \end{bmatrix}, \\ \mathbf{U}_e \triangleq \begin{bmatrix} \mathbf{G} \\ -\mathbf{I} \end{bmatrix}, \; \mathbf{L}_e \triangleq \begin{bmatrix} \mathbf{0}_{3\times4} \\ -\mathbf{K}_t \end{bmatrix} \end{cases} \tag{22}$$

$$\mathbf{M}_e \ddot{\mathbf{q}}(t) = \mathbf{K}_e \mathbf{q}(t) + \mathbf{B}_e \dot{\mathbf{q}}(t) + \mathbf{U}_e \mathbf{u}_f(t) + \mathbf{L}_e \mathbf{w}_f(t) \tag{23}$$

$$\dot{\mathbf{x}}_f(t) = \mathbf{A}_f \mathbf{x}_f(t) + \mathbf{B}_{1f} \mathbf{w}_f(t) + \mathbf{B}_{2f} \mathbf{u}_f(t) \tag{24}$$

$$\begin{cases} \mathbf{A}_f = \begin{bmatrix} \mathbf{0}_{7\times7} & \mathbf{I}_{7\times7} \\ \mathbf{M}_e^{-1}\mathbf{K}_e & \mathbf{M}_e^{-1}\mathbf{C}_e \end{bmatrix}, \\ \mathbf{B}_{1f} = \begin{bmatrix} \mathbf{0}_{7\times4} \\ \mathbf{M}_e^{-1}\mathbf{L}_e \end{bmatrix}, \\ \mathbf{B}_{2f} = \begin{bmatrix} \mathbf{0}_{7\times4} \\ \mathbf{M}_e^{-1}\mathbf{U}_e \end{bmatrix} \end{cases} \tag{25}$$

$$\begin{cases} \mathbf{\Phi}_f \equiv e^{\mathbf{A}_f T_s} \approx \mathbf{I} + \mathbf{A}_f \cdot T_s \\ \mathbf{\Gamma}_f \equiv \left(\int_0^{T_s} \mathbf{\Phi}_f(\tau)\, d\tau \right) \mathbf{B}_{1f} \approx \mathbf{B}_{1f} \cdot T_s \\ \mathbf{\Omega}_f \equiv \left(\int_0^{T_s} \mathbf{\Phi}_f(\tau)\, d\tau \right) \mathbf{B}_{2f} \approx \mathbf{B}_{2f} \cdot T_s \end{cases} \tag{26}$$

$$\mathbf{x}_f(k+1) = \mathbf{\Phi}_f \mathbf{x}_f(k) + \mathbf{\Gamma}_f \mathbf{w}_f(k) + \mathbf{\Omega}_f \mathbf{u}_f(k) \tag{27}$$

LQ objective function for the full-car model is defined as (28). The weights $1/\rho_i^2$ can be set by Bryson's rule, just as (8) [31]. The LQ objective function, (28), is converted into the vector-matrix form, (29), with the weighting matrices, $\mathbf{Q}_f$, $\mathbf{N}_f$ and $\mathbf{R}_f$. LQR is a full-state feedback controller, as given in (30), which minimizes J_f. The gain matrix $\mathbf{K}_f$ of LQR is obtained by solving Riccati equation comprising Φ_f, Ω_f, $\mathbf{Q}_f$, $\mathbf{N}_f$ and $\mathbf{R}_f$. Let denote this controller as LQRf1.

$$J_f = \sum_{k=0}^{\infty} \left\{ \begin{aligned} &\frac{1}{\rho_1^2} \ddot{z}_c^2(k) + \frac{1}{\rho_2^2} \sum_{i=1}^{4} \left\{ z_{si}(k) - z_{ui}(k) \right\}^2 \\ &+ \frac{1}{\rho_3^2} \sum_{i=1}^{4} z_{ui}^2(k) + \frac{1}{\rho_4^2} \sum_{i=1}^{4} u_i^2(k) \\ &+ \frac{1}{\rho_5^2} \ddot{\phi}^2(k) + \frac{1}{\rho_6^2} \dot{\phi}^2(k) + \frac{1}{\rho_7^2} \phi^2(k) \\ &+ \frac{1}{\rho_8^2} \ddot{\theta}^2(k) + \frac{1}{\rho_9^2} \dot{\theta}^2(k) + \frac{1}{\rho_{10}^2} \theta^2(k) \end{aligned} \right\} \tag{28}$$

$$J_f = \sum_{k=0}^{\infty} \begin{bmatrix} \mathbf{x}_f(k) \\ \mathbf{u}_f(k) \end{bmatrix}^T \begin{bmatrix} \mathbf{Q}_f & \mathbf{N}_f \\ \mathbf{N}_f^T & \mathbf{R}_f \end{bmatrix} \begin{bmatrix} \mathbf{x}_f(k) \\ \mathbf{u}_f(k) \end{bmatrix} \tag{29}$$

$$\mathbf{u}_f(k) = -\mathbf{K}_f \mathbf{x}_f(k) \tag{30}$$

By setting $\rho_5 \sim \rho_{10}$ to infinity, the LQ objective function (28) is reduced into (31), which has the same terms as (8). The LQ objective function, (31), is converted into the vector-matrix form, (32), with the weighting matrices, $\mathbf{Q}_{fq}$, $\mathbf{N}_{fq}$ and $\mathbf{R}_{fq}$. It is easy to obtain $\mathbf{K}_f$ by solving Riccati equation comprising $\mathbf{Q}_{fq}$, $\mathbf{N}_{fq}$ and $\mathbf{R}_{fq}$. Let denote this controller as LQRf2.

$$J_{fq} = \sum_{k=0}^{\infty} \left\{ \begin{aligned} &\frac{1}{\rho_1^2} \ddot{z}_c^2(k) + \frac{1}{\rho_2^2} \sum_{i=1}^{4} \left\{ z_{si}(k) - z_{ui}(k) \right\}^2 \\ &+ \frac{1}{\rho_3^2} \sum_{i=1}^{4} z_{ui}^2(k) + \frac{1}{\rho_4^2} \sum_{i=1}^{4} u_i^2(k) \end{aligned} \right\} \tag{31}$$

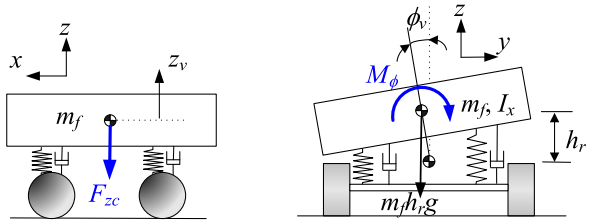

(a) 1-DOF heave model (b) 1-DOF roll model

(c) 1-DOF pitch model

FIGURE 4. Simple 1-DOF models describing heave, roll and pitch motions of a sprung mass.

$$J_{fq} = \sum_{k=0}^{\infty} \begin{bmatrix} \mathbf{x}_f(k) \\ \mathbf{u}_f(k) \end{bmatrix}^T \begin{bmatrix} \mathbf{Q}_{fq} & \mathbf{N}_{fq} \\ \mathbf{N}_{fq}^T & \mathbf{R}_{fq} \end{bmatrix} \begin{bmatrix} \mathbf{x}_f(k) \\ \mathbf{u}_f(k) \end{bmatrix} \tag{32}$$

A LQR requires full-state feedback. Hence, it is required that all state variables should be available for feedback. As shown in (16), there are 14 state variables in the full-car model. The dimension of $\mathbf{K}_f$, given in (30), is 4×14. Hence, 14 state variables must be measured or estimated for $\mathbf{K}_f$. However, it is very difficult to measure or estimate those variables with sensors in actual vehicles. For this reason, it is required to design a controller with a smaller number of state variables and gain elements. In the previous research, the controller $\mathbf{K}_q$ of (11) is used to derive $\mathbf{K}_f$ [21], [22]. The procedure of how to derive $\mathbf{K}_f$ from $\mathbf{K}_q$ can be found in the previous studies [21], [22]. Let denote the full-state feedback controller for the full-car model derived from $\mathbf{K}_q$ as LQRfq.

B. CONTROLLER DESIGN WITH SIMPLE 1-DOF MODELS

In the previous study, 3-DOF reference model was adopted to describe three motions, i.e., heave, roll and pitch motions of a sprung mass [27]. In the model, three motions were coupled with one another. In other words, there are cross-coupling terms on stiffness and damping matrices in the equations of motions under the basic assumption that the sprung mass is a rigid body. On the other hand, three separated 1-DOF models describing heave, roll and pitch motions are adopted in this paper. Fig. 4 shows three 1-DOF models, which describe the heave, roll and pitch motions of the sprung mass. In Fig. 4, F_{zc}, M_ϕ and M_θ are the vertical force, roll and pitch moments needed to control the corresponding motion of the sprung mass, respectively. Different from the model used in the previous study, these models have coupling terms among them.

The equations of motion for 1-DOF models are given in (33). In (33), F_{zc}, M_ϕ and M_θ, are the control inputs of the 1-DOF heave, roll and pitch models, respectively. The parameters of three 1-DOF models are calculated as (34) from the geometry and those of springs and dampers in the full-car model in Fig. 3.

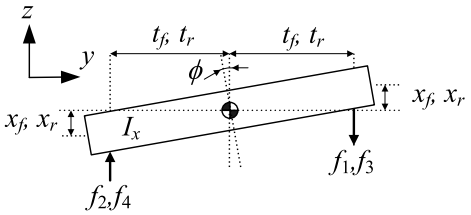

FIGURE 5. Free body diagram of 1-DOF roll model.

$$\begin{cases} m_s\ddot{z}_v + C_z\dot{z}_v + K_z z_v = F_{zc} \\ I_x\ddot{\phi}_v + C_\phi\dot{\phi}_v + K_\phi\phi_v - m_s g h_r \phi_v = M_\phi \\ I_y\ddot{\theta}_v + C_\theta\dot{\theta}_v + K_\theta\theta_v - m_s g h_p \theta_v = M_\theta \end{cases} \tag{33}$$

$$\begin{cases} K_z = k_{s1} + k_{s2} + k_{s3} + k_{s4} \\ C_z = b_{s1} + b_{s2} + b_{s3} + b_{s4} \\ K_\phi = t_f^2(k_{s1} + k_{s2}) + t_r^2(k_{s3} + k_{s4}) \\ C_\phi = t_f^2(b_{s1} + b_{s2}) + t_r^2(b_{s3} + b_{s4}) \\ K_\theta = l_f^2(k_{s1} + k_{s2}) + l_r^2(k_{s3} + k_{s4}) \\ C_\theta = l_f^2(b_{s1} + b_{s2}) + l_r^2(b_{s3} + b_{s4}) \end{cases} \tag{34}$$

The procedure how to derive K_ϕ, C_ϕ, K_θ and C_θ is explained. Fig. 5 shows the free body diagram of 1-DOF roll model. In Fig. 5, x_f and x_r are the vertical displacement of the sprung mass at each corner caused by roll motion. The equation of roll motion is derived as (35). x_f and x_r are calculated as (36) from the geometry. The suspension forces acting on the sprung mass are calculated as (37) from (12) and (36). By replacing f_i of (35) with those of (37), (35) is rearranged into (38). From (38), K_ϕ and C_ϕ are obtained as (34). With the same manner, K_θ and C_θ of 1-DOF pitch model are calculated as (34).

$$\begin{aligned} I_x\ddot{\phi} &= t_f f_1 + t_r f_3 + t_f f_2 + t_r f_4 \\ &= t_f(f_1 + f_2) + t_r(f_3 + f_4) \end{aligned} \tag{35}$$

$$\begin{cases} x_f = t_f \sin\phi \approx t_f\phi \\ x_r = t_r \sin\phi \approx t_r\phi \end{cases} \tag{36}$$

$$\begin{cases} f_1 = -k_{s1}x_f - b_{s1}\dot{x}_f = -k_{s1}t_f\phi - b_{s1}t_f\dot{\phi} \\ f_2 = -k_{s2}x_f - b_{s2}\dot{x}_f = -k_{s2}t_f\phi - b_{s2}t_f\dot{\phi} \\ f_3 = -k_{s3}x_r - b_{s3}\dot{x}_r = -k_{s3}t_r\phi - b_{s3}t_r\dot{\phi} \\ f_4 = -k_{s4}x_r - b_{s4}\dot{x}_r = -k_{s4}t_r\phi - b_{s4}t_r\dot{\phi} \end{cases} \tag{37}$$

$$\begin{aligned} I_x\ddot{\phi} &= t_f \cdot \left\{-k_{s1}t_f\phi - b_{s1}t_f\dot{\phi} - k_{s2}t_f\phi - b_{s2}t_f\dot{\phi}\right\} \\ &\quad + t_r \cdot \left\{-k_{s3}t_r\phi - b_{s3}t_r\dot{\phi} - k_{s4}t_r\phi - b_{s4}t_r\dot{\phi}\right\} \\ &= t_f^2\left\{-(k_{s1} + k_{s2})\phi - (b_{s1} + b_{s2})\dot{\phi}\right\} \\ &\quad + t_r^2\left\{-(k_{s3} + k_{s4})\phi - (b_{s3} + b_{s4})\dot{\phi}\right\} \\ &= -\left\{t_f^2(k_{s1} + k_{s2}) + t_r^2(k_{s3} + k_{s4})\right\}\phi \\ &\quad - \left\{t_f^2(b_{s1} + b_{s2}) + t_r^2(b_{s3} + b_{s4})\right\}\dot{\phi} \\ &= -K_\phi\phi - C_\theta\dot{\phi} \end{aligned} \tag{38}$$

For controller design, the state-space equations of these models are needed. The state-space equation of the 1-DOF heave model is derived as an example. The state variables of 1-DOF heave model are defined as (39). With the definition, the state-space equation is derived as (40). Under the assumption that the sampling time is T_s, the discrete-time state-space equation of 1-DOF heave model is obtained as (41). In (41), the definitions of the matrices Φ_z, Γ_z, and Ω_z are calculated by the identical way to (6). For the 1-DOF roll and pitch models, the identical procedure can be applied with the definitions of state variables, given in (42), in order to obtain the discrete-time state-space equations as (43).

$$\mathbf{x}_z(t) \equiv \begin{bmatrix} z_v(t) & \dot{z}_v(t) \end{bmatrix}^T \tag{39}$$

$$\begin{aligned} \dot{\mathbf{x}}_z(t) &= \mathbf{A}_z\mathbf{x}_z(t) + \mathbf{B}_{2z}F_{zc}(t) \\ &= \begin{bmatrix} 0 & 1 \\ -\frac{K_z}{m_s} & -\frac{C_z}{m_s} \end{bmatrix}\mathbf{x}(t) + \begin{bmatrix} 0 \\ \frac{1}{m_s} \end{bmatrix}F_{zc}(t) \end{aligned} \tag{40}$$

$$\mathbf{x}_z(k+1) = \mathbf{\Phi}_z\mathbf{x}_z(k) + \mathbf{\Omega}_z F_{zc}(k) \tag{41}$$

$$\begin{cases} \mathbf{x}_\phi(t) \equiv \begin{bmatrix} \phi_v(t) & \dot{\phi}_v(t) \end{bmatrix}^T \\ \mathbf{x}_\theta(t) \equiv \begin{bmatrix} \theta_v(t) & \dot{\theta}_v(t) \end{bmatrix}^T \end{cases} \tag{42}$$

$$\begin{cases} \mathbf{x}_\phi(k+1) = \mathbf{\Phi}_\phi\mathbf{x}_\phi(k) + \mathbf{\Omega}_\phi M_\phi(k) \\ \mathbf{x}_\theta(k+1) = \mathbf{\Phi}_\theta\mathbf{x}_\theta(k) + \mathbf{\Omega}_\theta M_\theta(k) \end{cases} \tag{43}$$

With the discrete-time state-space equations of (41) and (43), LQR is designed. The LQ objective functions are defined as (44), (45) and (46) for the 1-DOF vertical, roll and pitch models, respectively. The full-state feedback controllers or the control inputs of these models are defined as (47). The controller gain matrices, $\mathbf{K}_{LQR,z}$, $\mathbf{K}_{LQR,\phi}$ and $\mathbf{K}_{LQR,\theta}$, in (47) are calculated by solving Riccati equations with the matrices in the state-space equations and LQ objective functions.

$$\begin{aligned} J_z &= \sum_{k=0}^{\infty}\left\{\frac{1}{\zeta_1^2}\ddot{z}_v^2(k) + \frac{1}{\zeta_1^2}F_{zc}^2(k)\right\} \\ &= \sum_{k=0}^{\infty}\begin{bmatrix} \mathbf{x}_z(k) \\ F_{zc}(k) \end{bmatrix}^T\begin{bmatrix} \mathbf{Q}_z & \mathbf{N}_z \\ \mathbf{N}_z^T & \mathbf{R}_z \end{bmatrix}\begin{bmatrix} \mathbf{x}_z(k) \\ F_{zc}(k) \end{bmatrix} \end{aligned} \tag{44}$$

$$\begin{aligned} J_\phi &= \sum_{k=0}^{\infty}\left\{\frac{1}{\xi_1^2}\phi_v^2(k) + \frac{1}{\xi_2^2}\dot{\phi}_v^2(k) + \frac{1}{\xi_3^2}M_\phi^2(k)\right\} \\ &= \sum_{k=0}^{\infty}\begin{bmatrix} \mathbf{x}_\phi(k) \\ M_\phi(k) \end{bmatrix}^T\begin{bmatrix} \mathbf{Q}_\phi & \mathbf{N}_\phi \\ \mathbf{N}_\phi^T & \mathbf{R}_\phi \end{bmatrix}\begin{bmatrix} \mathbf{x}_\phi(k) \\ M_\phi(k) \end{bmatrix} \end{aligned} \tag{45}$$

$$\begin{aligned} J_\theta &= \sum_{k=0}^{\infty}\left\{\frac{1}{\sigma_1^2}\theta_c^2(k) + \frac{1}{\sigma_2^2}\dot{\theta}_c^2(k) + \frac{1}{\sigma_3^2}M_\theta^2(k)\right\} \\ &= \sum_{k=0}^{\infty}\begin{bmatrix} \mathbf{x}_\theta(k) \\ M_\theta(k) \end{bmatrix}^T\begin{bmatrix} \mathbf{Q}_\theta & \mathbf{N}_\theta \\ \mathbf{N}_\theta^T & \mathbf{R}_\theta \end{bmatrix}\begin{bmatrix} \mathbf{x}_\theta(k) \\ M_\theta(k) \end{bmatrix} \end{aligned} \tag{46}$$

$$\begin{cases} F_{zc}(k) = -\mathbf{K}_{LQR,z}\mathbf{x}_z(k) \\ M_\phi(k) = -\mathbf{K}_{LQR,\phi}\mathbf{x}_\phi(k) \\ M_\theta(k) = -\mathbf{K}_{LQR,\theta}\mathbf{x}_\theta(k) \end{cases} \tag{47}$$

For sliding mode controller design, the sliding surface for the 1-DOF heave model is defined as (48). To make the sliding surface be zero, the convergence condition is given in (49). However, the condition (49) is so severe that the control input obtained from it becomes quite large. As a result, responses of a vehicle with the controller designed with (49) show severe chattering phenomena [32]. To avoid the case, the new relaxed convergence condition (50) is used. Generally, a necessary and sufficient condition for the existence and the sliding motion and the convergence of sliding surface onto hyperplane is given as (51). Evidently, the new condition, (50), satisfies (51) [33]. In (50), α_z is the parameter used to tune the convergence speed. If α_z becomes smaller, the convergence speed gets faster and the control input does larger. According to the previous study, there is chattering in the responses of a vehicle and the control input of the controller if α_z is set to 0.3 or less in spite of better control performance [32]. By combining (41), (48) and (50), the equation (52) is obtained. From (52), the vertical force F_{zc} is calculated as (53). In (53), $()^+$ represents the pseudo-inverse. With this manner, the control roll moment M_ϕ and the control pitch moment M_θ can be easily derived as (54). For closed-loop stability, the tuning parameters, α_z, α_ϕ and α_θ, should be less than 1.

$$\mathbf{s}_z(k) = \mathbf{H}\mathbf{x}_z(k) \tag{48}$$

$$\mathbf{s}_z(k+1) = \mathbf{s}_z(k) = 0 \tag{49}$$

$$\mathbf{s}_z(k+1) = \alpha_z\mathbf{s}_z(k) \quad (0 < \alpha_z < 1) \tag{50}$$

$$|\mathbf{s}_z(k+1)| < |\mathbf{s}_z(k)| \tag{51}$$

$$\mathbf{s}_z(k+1) = \mathbf{H}\mathbf{\Phi}_z\mathbf{x}_z(k) + \mathbf{H}\mathbf{\Omega}_z F_{zc}(k) = \alpha_z\mathbf{H}\mathbf{x}_z(k) \tag{52}$$

$$\begin{aligned} F_{zc}(k) &= -\left(\mathbf{H}\mathbf{\Omega}_z\right)^+\mathbf{H}\left(\mathbf{\Phi}_z - \alpha_z\mathbf{I}\right)\mathbf{x}_z(k) \\ &= -\mathbf{\Omega}_z^+\left(\mathbf{\Phi}_z - \alpha_z\mathbf{I}\right)\mathbf{x}_z(k) \\ &= -\mathbf{K}_{SMC,z}\mathbf{x}(k) \end{aligned} \tag{53}$$

$$\begin{cases} M_\phi(k) = -\mathbf{\Omega}_\phi^+\left(\mathbf{\Phi}_\phi - \alpha_\phi\mathbf{I}\right)\mathbf{x}_\phi(k) \\ = -\mathbf{K}_{SMC,\phi}\mathbf{x}_\phi(k) \\ M_\theta(k) = -\mathbf{\Omega}_\theta^+\left(\mathbf{\Phi}_\theta - \alpha_\theta\mathbf{I}\right)\mathbf{x}_\theta(k) \\ = -\mathbf{K}_{SMC,\theta}\mathbf{x}_\theta(k) \end{cases} \tag{54}$$

The control inputs, i.e., F_{zc}, M_ϕ and M_θ, obtained from (47) and (54), are converted into the active forces, u_1, u_2, u_3, and u_4, using the input decoupling transformation, given in (15), as (55) [25]. This is called modal control or Lotus Modal Control (LMC) [24,30]. In (55), $\mathbf{G}^+$ is the pseudo-inverse of $\mathbf{G}$. The control inputs, F_{zc}, M_ϕ and M_θ, are stable because those are designed by LQR and SMC. The magnitudes of the singular values of $\mathbf{G}^+$ are less than 1. In view of the small gain theorem, F_{zc}, M_ϕ and M_θ are not amplified by $\mathbf{G}^+$. For this reason, the control inputs at each corner, i.e., u_1, u_2, u_3 and u_4, obtained with $\mathbf{G}^+$ from F_{zc}, M_ϕ and M_θ are also stable.

$$\mathbf{u}_f(k) = \mathbf{G}^+\begin{bmatrix} F_{zc}(k) \\ M_\phi(k) \\ M_\theta(k) \end{bmatrix}$$

$$= -\mathbf{G}^{+}\begin{bmatrix}\mathbf{K}_{FB,z} & \mathbf{0}_{1\times2} & \mathbf{0}_{1\times2}\\ \mathbf{0}_{1\times2} & \mathbf{K}_{FB,\phi} & \mathbf{0}_{1\times2}\\ \mathbf{0}_{1\times2} & \mathbf{0}_{1\times2} & \mathbf{K}_{FB,\theta}\end{bmatrix}\begin{bmatrix}\mathbf{x}_z(k)\\ \mathbf{x}_\phi(k)\\ \mathbf{x}_\theta(k)\end{bmatrix}$$
$$= -\mathbf{G}^{+}\mathbf{K}_{FB}\begin{bmatrix}\mathbf{x}_z(k)\\ \mathbf{x}_\phi(k)\\ \mathbf{x}_\theta(k)\end{bmatrix} \quad (55)$$

In (55), the gain matrices, $\mathbf{K}_{FB,z}$, $\mathbf{K}_{FB,\phi}$ and $\mathbf{K}_{FB,\theta}$ can be replaced with $\mathbf{K}_{LQR,z}$, $\mathbf{K}_{LQR,\phi}$ and $\mathbf{K}_{LQR,\theta}$ of (47) or with $\mathbf{K}_{SMC,z}$, $\mathbf{K}_{SMC,\phi}$ and $\mathbf{K}_{SMC,\theta}$ of (54). Let denote the controller with the gain matrices $\mathbf{K}_{LQR,z}$, $\mathbf{K}_{LQR,\phi}$ and $\mathbf{K}_{LQR,\theta}$ of (47) as the modal LQR or MDLQR. Let denote the controller with the gain matrices $\mathbf{K}_{SMC,z}$, $\mathbf{K}_{SMC,\phi}$ and $\mathbf{K}_{SMC,\theta}$ of (47) as the modal SMC or MDSMC.

As shown in (55), six gain elements in $\mathbf{K}_{FB}$ are needed for MDLQR and MDSMC. On the contrary, LQR with the full-car model, i.e., $\mathbf{K}_f$ in (30), requires 56 gain elements for full-state feedback. Moreover, six state variables are required for the feedback controllers, i.e., MDLQR and MDSMC, as shown in (55). On the other hand, LQR with the full-car model requires 14 state variables for full-state feedback. Therefore, MDLQR and MDSMC are much simpler and easier to implement.

C. DESIGN OF STRUCTURED LQ STATIC OUTPUT FEEDBACK CONTROLLER

The controller (55) represents the form of structured static output feedback in terms of 7-DOF full-car model, given in (55). The controller (55) can be rewritten as (56). The feedback controller in (56) is the form of the static output feedback (SOF) control [21], [22], [34]–[37]. The controller gain matrix $\mathbf{K}_{FB}$ of (56) can be rewritten as (57). As shown in (56) and (57), the available outputs for the structured SOF control are the vertical position and velocity, the roll angle, the roll rate, the pitch angle, and the pitch rate of the sprung mass, as given in (39) and (42). These outputs can be selected from the state $\mathbf{x}_f$, given in (16), with the output matrix $\mathbf{C}_f$. To derive $\mathbf{C}_f$, new vectors are defined as (58). With those vectors, $\mathbf{C}_f$ is derived as (59).

$$\mathbf{u}_f = -\mathbf{G}^{+}\mathbf{K}_{FB}\begin{bmatrix}\mathbf{x}_z(k)\\ \mathbf{x}_\phi(k)\\ \mathbf{x}_\theta(k)\end{bmatrix} = -\mathbf{G}^{+}\mathbf{K}_{FB}\mathbf{C}_f\,\mathbf{x}_f(k)$$
$$= -\mathbf{K}_{FBS}\mathbf{x}_f(k) \quad (56)$$

$$\mathbf{K}_{FB} \equiv \begin{bmatrix}\mathbf{K}_{FB,z} & \mathbf{0}_{1\times2} & \mathbf{0}_{1\times2}\\ \mathbf{0}_{1\times2} & \mathbf{K}_{FB,\phi} & \mathbf{0}_{1\times2}\\ \mathbf{0}_{1\times2} & \mathbf{0}_{1\times2} & \mathbf{K}_{FB,\theta}\end{bmatrix}$$
$$= \begin{bmatrix}K_{v1} & K_{v2} & 0 & 0 & 0 & 0\\ 0 & 0 & K_{r1} & K_{r2} & 0 & 0\\ 0 & 0 & 0 & 0 & K_{p1} & K_{p2}\end{bmatrix} \quad (57)$$

$$\mathrm{Z} \triangleq \begin{bmatrix}1 & 0 & 0\end{bmatrix},\quad \Phi \triangleq \begin{bmatrix}0 & 1 & 0\end{bmatrix},$$
$$\Theta \triangleq \begin{bmatrix}0 & 0 & 1\end{bmatrix} \quad (58)$$

$$\mathbf{C}_f \equiv \begin{bmatrix}\mathrm{Z} & \mathbf{0}_{1\times4} & \mathbf{0}_{1\times7}\\ \mathbf{0}_{1\times7} & \mathrm{Z} & \mathbf{0}_{1\times4}\\ \Phi & \mathbf{0}_{1\times4} & \mathbf{0}_{1\times7}\\ \mathbf{0}_{1\times7} & \Phi & \mathbf{0}_{1\times4}\\ \Theta & \mathbf{0}_{1\times4} & \mathbf{0}_{1\times7}\\ \mathbf{0}_{1\times7} & \Theta & \mathbf{0}_{1\times4}\end{bmatrix} \quad (59)$$

Different from MDLQR and MDSMC, the six gain elements in $\mathbf{K}_{FB}$ can be optimized with the LQ objective function, **(31)**. In other words, the six gain elements in $\mathbf{K}_{FB}$ should be determined in order to design the LQ SOF controller. If these elements can be found to minimize the LQ objective function (28) using some heuristic optimization methods, then it is the optimal LQ SOF controller. This problem is formulated as the optimization one, (60). In (60), eig($\mathbf{X}$) and mag(y) are the operators used to calculate the eigenvalues of the matrix $\mathbf{X}$ and the magnitudes of the complex numbers y, respectively. In this paper, the evolutionary strategy, CMA-ES, is used to find the optimum $\mathbf{K}_{FBS}$ [38]. The stability of the closed-loop system with $\mathbf{K}_{FBS}$ is guaranteed by solving (60) because the objective function J_{fs} cannot be calculated if the closed-system is unstable. Let denote this structured LQ SOF controller as SLQSOF.

$$\min_{\mathbf{K}_{FB}} J_{fs} = \frac{1}{2}\mathrm{trace}\left(\mathbf{P}_s\right), \quad \mathbf{P}_s = \mathbf{P}_s^T > 0$$
$$s.t.\ \begin{cases}\max\left\{\mathrm{mag}\left(\mathrm{eig}\left[\mathbf{\Phi}_f - \mathbf{\Omega}_f\mathbf{K}_{FBS}\right]\right)\right\} < 1\\ \left(\mathbf{\Phi}_f - \mathbf{\Omega}_f\mathbf{K}_{FBS}\right)^T\mathbf{P}_s\left(\mathbf{\Phi}_f - \mathbf{\Omega}_f\ \mathbf{K}_{FBS}\right) - \mathbf{P}_s\\ +\mathbf{Q}_{fq} - \mathbf{K}_{FBS}^T\mathbf{N}_{fq}^T - \mathbf{N}_{fq}\mathbf{K}_{FBS} + \mathbf{K}_{FBS}^T\mathbf{R}_{fq}\ \mathbf{K}_{FBS} = 0\end{cases} \quad (60)$$

As shown in (44), (45) and (46), the tuning parameters of MDLQR are ζ_i, ξ_i and σ_i. So, there are eight tuning parameters in designing MDLQR. For MDSMC, there is a single tuning parameter, α. On the other hand, the tuning parameters of SLQSOF are the weights ρ_i in the LQ objective function, (31). So, there are four tuning parameters in SLQSOF. In terms of the number of tuning parameters, MDSMC is the simplest controller among those controllers.

III. SIMULATION

In this section, analysis on frequency responses and simulation are performed to evaluate the performance of the designed controllers, MDLQR, MDSMC and SLQSOF. Through frequency response analysis, five controllers, LQRf2, LQRfq, MDLQR, MDSMC and SLQSOF, are compared to one another. In the previous work, it was shown that LQRf2 and LQRfq are equivalent to each other [22]. So, these controllers are used as a base one for comparison.

Table 1 shows the parameters of 7-DOF full-car and 1-DOF simple models, which were referred from Demo_Lexus_NX300h given in CarMaker. LQRf2 and LQRfq are designed with the weights given in Table 2. To avoid the chattering in control responses, the values of the tuning parameters, α_z, α_ϕ and α_θ, in MDSMC are set to 0.6.

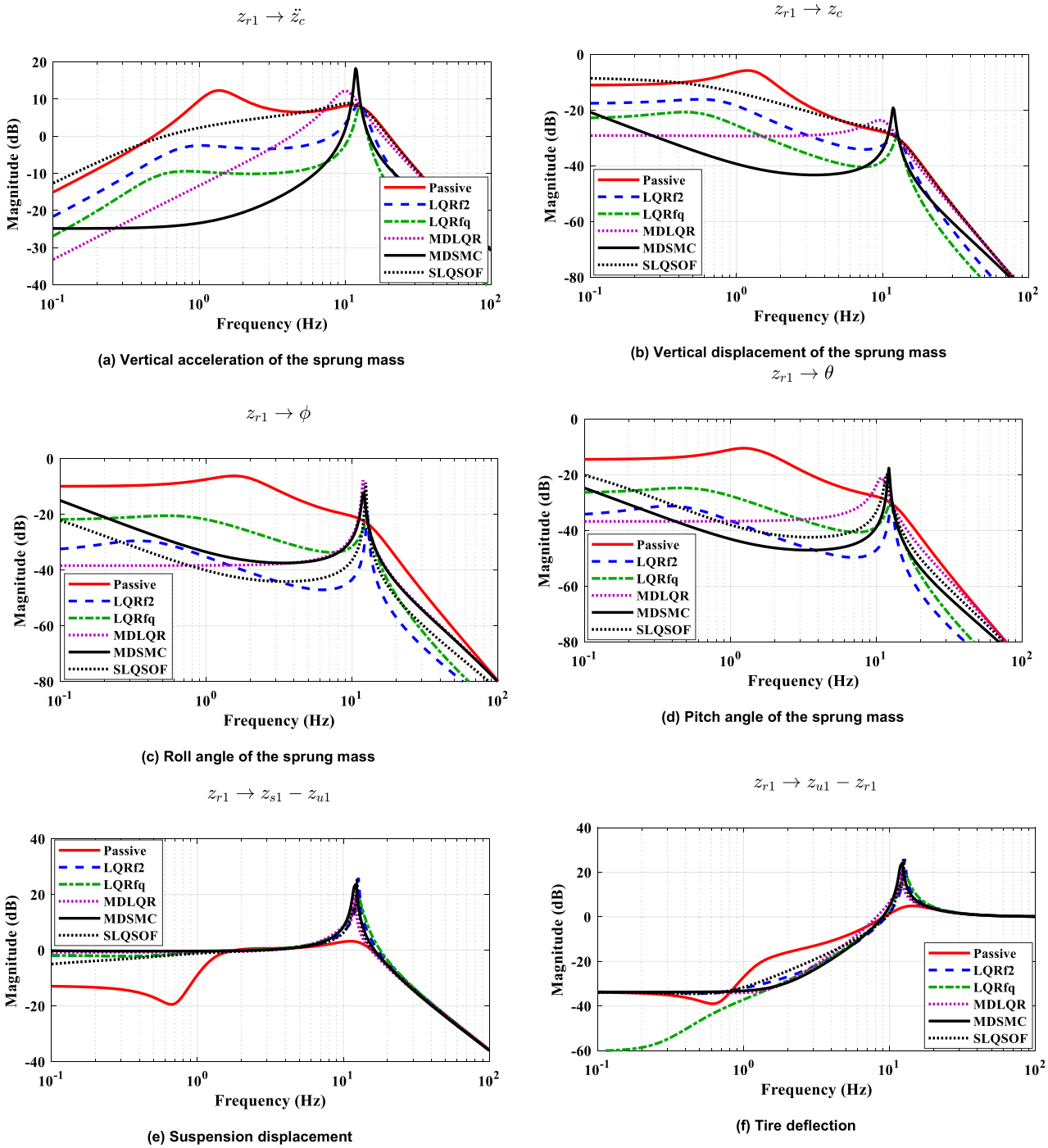

FIGURE 6. Frequency responses from the road profile to each output.

Table 3 shows the largest magnitudes of the eigenvalues of the closed-loop system with the designed controllers. For stability, the largest magnitude of the eigenvalues of the discrete-time closed-loop system should be less than 1. As shown in Table 3, all the designed controllers are stable because the largest magnitudes of the eigenvalues are smaller than 1.

A. ANALYSIS ON REQUENCY RESPONSES

To check the effects of MDLQR, MDSMC and SLQSOF on ride comfort, singular value plots were drawn from the road profile into several outputs. To draw the plots for these controllers, the state-space equation of the full-car model, (27), with the parameters given in Table 1 was used.

Fig. 6 shows singular value plots from the road profile into several outputs. In these plots, the outputs are those of the sprung mass, the suspension displacement and the tire deflection. As shown in Fig. 6-(a), MDSMC show the best performance in controlling the vertical acceleration of the sprung mass. This means that MDSMC can provide good ride comfort. Moreover, MDLQR is also effective for ride

TABLE 1. Parameter descriptions of its values of the 2-DOF quarter-car and 7-DOF full-car models.

m_f	1,950.0 kg	m_q	$m_f/4$
m_{u1}, m_{u2}, m_{u3}, m_{u4}	62.0 kg		
I_x	703.7 kg·m^2	I_y	2,358.0 kg·m^2
k_{s1}, k_{s2}	35,000 N/m	k_{s3}, k_{s4}	45,000 N/m
c_{s1}, c_{s2}, c_{s3}, c_{s4}	3,500 N·s/m	k_{t1}, k_{t2}, k_{t3}, k_{t4}	391,961 N/m
k_s	35,000 N/m	c_s	3,500 N·s/m
k_t	391,961 N/m	t_f, t_r	0.785 m
l_f	1.172 m	l_r	1.488 m

TABLE 2. Maximum allowable values in LQ cost function.

η_1	1.0 m/s^2	η_2	0.2 m	η_3	0.2 m
η_4	3,000 N	η_5	10 deg/s^2	η_6	10 deg/s^2
η_7	2 deg	η_8	10 deg/s	η_9	2 deg
η_{10}	10 deg/s				

TABLE 3. Largest magnitudes of eigenvalues of the closed-loop systems with the designed controllers.

LQRf2	0.99924	LQRfq	0.99774
MDLQR	0.99892	MDSMC	0.99997
SLQSOF	0.99977		

comfort. Notable feature of MDLQR and MDSMC, i.e., a modal controller, is that those make ride comfort near 10Hz worse than the passive system, and that the resonant frequency of the tire was move to slightly lower. These are typical phenomena when using a modal controller [39]. On the other hand, SLQSOF shows worse performance in terms of ride comfort, compared to MDLQR and MDSMC. This tendency is also valid to the height of the sprung mass, as shown in Fig. 6-(b). As shown in Fig. 6-(c) and -(d), five controllers are nearly equivalent to one another in controlling the roll and pitch motions of the sprung mass. As a counter effect to good ride comfort, the suspension displacements were increased and the tire deflections decreased. This means that road holding was deteriorated by those controllers. Among those controllers, MDSMC shows the largest suspension displacement and the least tire deflection within the range from 2 to 10Hz as a result of the minimum vertical acceleration and height of the sprung mass. This is well-known trade-off between ride comfort and road holding. From the frequency response analysis, it can be concluded that MDSMC is the best controller in terms of ride comfort.

B. SIMULATION IN VEHICLE SIMULATION SOFTWARE WITH THE DESIGNED CONTROLLERS

Simulation was conducted on the vehicle simulation software, CarMaker, connected with MATLAB/Simulink. IPG CarMaker has been widely used for validation on vehicle stability and active/semi-active suspension control over the last decade [40]–[43]. The vehicle model used for simulation was Demo_Lexus_NX300h provided in CarMaker. Fig. 7 shows the single bump profile used for simulation. There were no

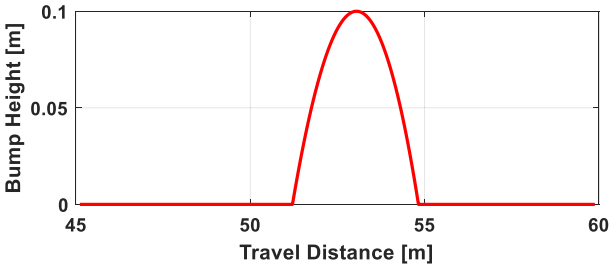

FIGURE 7. Bump profile.

TABLE 4. Peak-to-peak values of responses for each controller at front right corner.

	$\ddot{z}_c$ (m/s^2)	θ (deg)	SD (m)	TD (m)	Control input (N)
Passive	7.8	6.2	0.130	0.015	0
LQRfq	5.1	2.0	0.101	0.011	4557
MDLQR	2.5	0.4	0.099	0.008	5483
MDSMC	3.2	2.1	0.179	0.009	6050
SLQSOF	6.9	1.4	0.112	0.011	4185

actuator models in the simulation. In other words, an actuator used to generate a control force has infinite bandwidth and has no limits on the magnitude of it. The vehicle speed was set to 30km/h and maintained as it by a speed controller given in CarMaker. Then, the vehicle passes the bump. The tire-road friction coefficient is set to 0.85. There are no roll motions since the bump is evenly applied to left and right wheels.

Fig. 8 shows the simulation results for the designed controllers. As shown in Fig. 8-(a) and -(b), MDLQR shows the best performance in controlling the vertical acceleration and the pitch angle of the sprung mass. This is natural because MDLQR generates the largest control inputs, as shown in Fig. 8-(e). As a result, MDLQR gives the largest suspension displacement and the smallest tire deflection, as shown in Fig. 8-(c) and -(d). MDSMC shows relatively good performance in terms of ride comfort. These results are different from those presented in the frequency response of Fig. 6. On the other hand, SLQSOF shows good performance in controlling the pitch angle. However, it gives poor performance in controlling the vertical acceleration. This is opposite to LQRfq. LQRfq shows relatively poor performance in controlling the pitch angle because the LQ objective function of LQRfq has no terms on it.

Tables 4 and 5 show the peak-to-peak and root-mean-square values of the responses of Fig. 8 for each controller at front left corner, respectively. In Tables 4 and 4, SD and TD denotes the suspension displacement and the tire deflection at front left corner, respectively. As shown in Tables 4 and 5, MDLQR shows the best performance from the viewpoint of ride comfort. MDSMC can be also good choice for ride comfort. However, SLQSOF is not recommend because it cannot control the vertical acceleration of the sprung mass. These results are coincided with those given in Fig. 8.

Three controllers, MDLQR, MDSMC and SLQSOF, have the identical structure of (57). The difference among them is controller design methodology. So, it is not valid that these

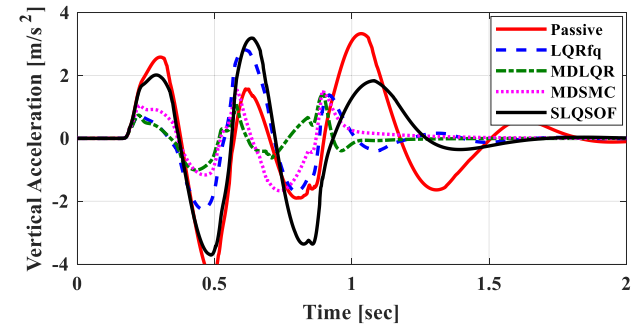

(a) Vehicle acceleration of the sprung mass

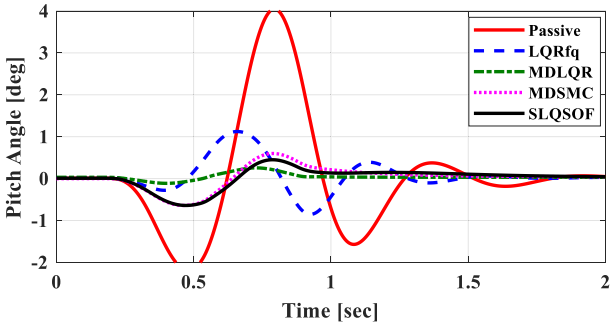

(b) Pitch angle of the sprung mass

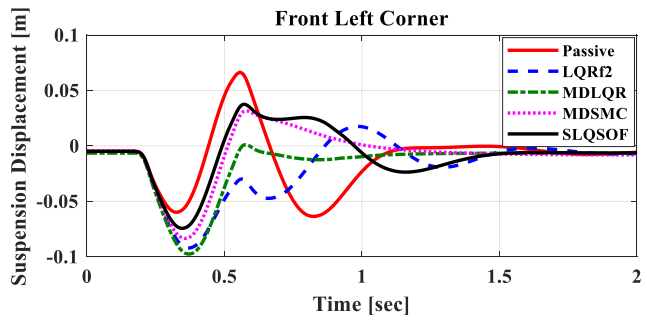

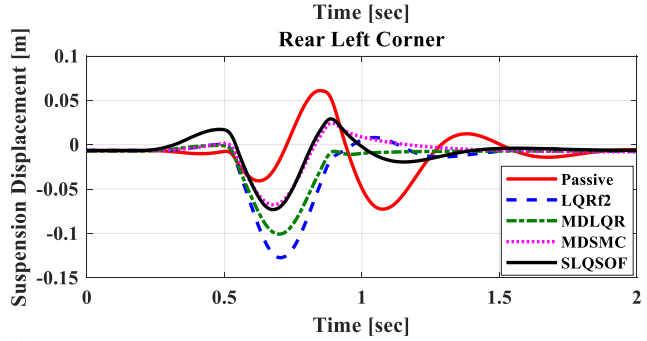

(c) Suspension displacement

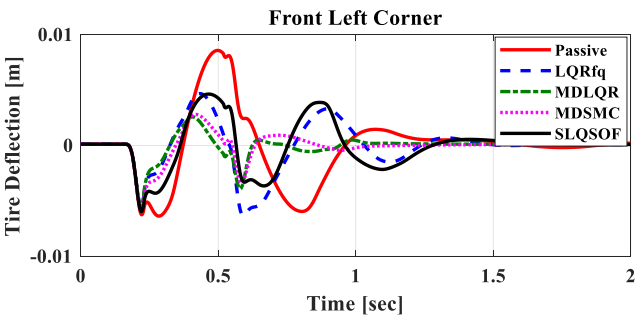

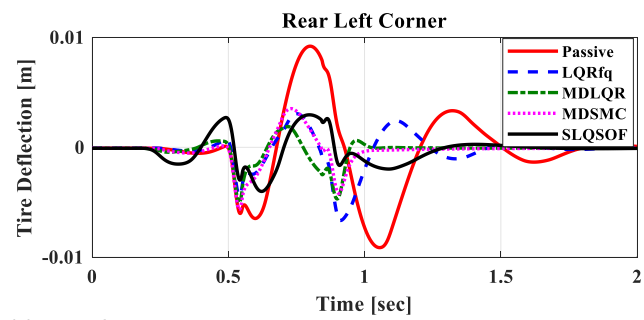

(d) Tire deflection

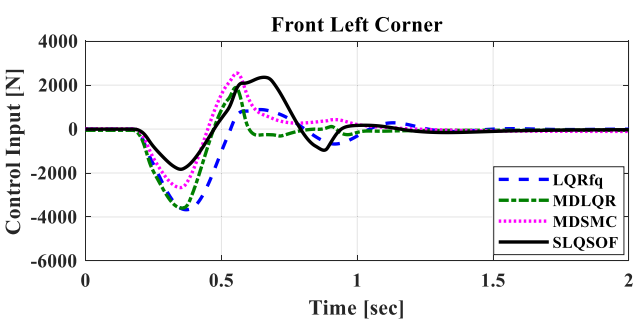

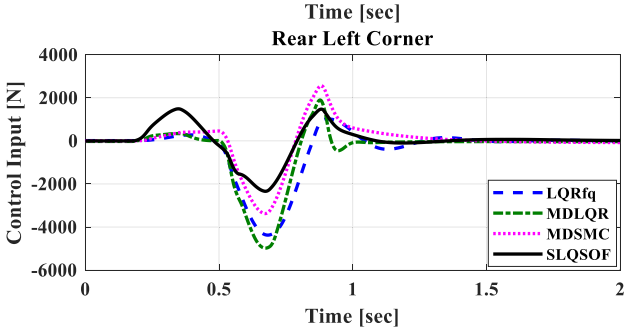

(e) Control input

FIGURE 8. Simulation results obtained from CarMaker for each controller.

TABLE 5. Root-mean-square values of responses for each controller at front right corner.

	$\ddot{z}_c$ (m/s^2)	θ (deg)	SD (m)	TD (m)	Control input (N)
Passive	1.56	1.39	0.029	0.003	0
LQRfq	0.91	0.40	0.031	0.002	1088
MDLQR	0.37	0.09	0.029	0.001	978
MDSMC	0.61	0.27	0.025	0.001	851
SLQSOF	1.48	0.25	0.025	0.002	826

controllers are compared with simulations under the identical condition. For example, the performance of MDSMC can be improved by decreasing the value of α. Moreover, the performance of SLQSOF can be improved by reducing the value of η_1 in (31).

The key point of this paper is to reduce the number of elements of the controller gain matrix, which is identical to that of signals used for feedback control. The number of the gain elements of LQRfq is 4, which means that it requires 4 signals for feedback control. On the contrary, the number of the gain elements of MDLQR, MDSMC and SLQSOF is 6. This is much smaller than that of LQRf2, i.e., 56. Moreover, MDLQR and MDSMC are much easier to design than LQRf2, LQRfq and SLQSOF.

IV. CONCLUSION

In this paper, the modal controller was derived from three controllers, i.e., heave, roll and pitch controllers, designed with three 1-DOF models describing the vertical, roll and pitch motions of the sprung mass. In the discrete-time domain, heave, roll and pitch controllers are designed with these 1-DOF models by applying discrete-time LQR and SMC. The control inputs of these controllers are converted into four ones at each corner in the full-car model with input decoupling transformation. The modal controller requires six state variables and has six gain elements. Hence, the number of gain elements of these controllers is much smaller than those of LQR for the full-car model. By the nature of structured and SOF control of the modal controller, the modal controller itself was designed by the heuristic optimization method, i.e., CMA-ES. Through a frequency response analysis and a simulation on the vehicle simulation package, the modal controllers designed with LQR and SMC show quite effective in controlling the motions of the sprung mass in terms of ride comfort. Further research will include the design of feedforward controller design with measured acceleration signals, which can improve the control performance against external disturbances.

REFERENCES

[1] H. E. Tseng and D. Hrovat, "State of the art survey: Active and semi-active suspension control," *Vehicle Syst. Dyn.*, vol. 53, no. 7, pp. 1034–1062, 2015, doi: 10.1080/00423114.2015.1037313.

[2] *Mechanical Vibration and Shock—Evaluation of Human Exposure to Whole-Body Vibration—Part 1: General Requirements*, ISO Standard 2631-1, International Organization for Standardization, Geneva, Switzerland, 1997.

[3] A. N. Rimell and N. J. Mansfield, "Design of digital filters for frequency weightings required for risk assessments of workers exposed to vibration," *Ind. Health*, vol. 45, no. 4, pp. 512–519, 2007, doi: 10.2486/indhealth.45.512.

[4] T. Tseng and D. Hrovat, "Some characteristics of optimal vehicle suspensions based on quarter-car models," in *Proc. 29th IEEE Conf. Decis. Control*, Dec. 1990, pp. 2232–2237, doi: 10.1109/CDC.1990.204022.

[5] D. Hrovat, "Survey of advanced suspension developments and related optimal control applications," *Automatica*, vol. 33, no. 10, pp. 1781–1817, 1997, doi: 10.1016/S0005-1098(97)00101-5.

[6] D. Cao, X. Song, and M. Ahmadian, "Editors' perspectives: Road vehicle suspension design, dynamics, and control," *Vehicle Syst. Dyn.*, vol. 49, nos. 1–2, pp. 3–28, Feb. 2011, doi: 10.1080/00423114.2010.532223.

[7] C. Poussot-Vassal, C. Spelta, O. Sename, S. M. Savaresi, and L. Dugard, "Survey and performance evaluation on some automotive semi-active suspension control methods: A comparative study on a single-corner model," *Annu. Rev. Control*, vol. 36, no. 1, pp. 148–160, Apr. 2012, doi: 10.1016/j.arcontrol.2012.03.011.

[8] J. Theunissen, A. Tota, P. Gruber, M. Dhaens, and A. Sorniotti, "Preview-based techniques for vehicle suspension control: A state-of-the-art review," *Annu. Rev. Control*, vol. 51, pp. 206–235, Jan. 2021, doi: 10.1016/j.arcontrol.2021.03.010.

[9] Y. Huang, J. Na, X. Wu, X. Liu, and Y. Guo, "Adaptive control of nonlinear uncertain active suspension systems with prescribed performance," *ISA Trans.*, vol. 54, pp. 145–155, Jan. 2015, doi: 10.1016/j.isatra.2014.05.025.

[10] R. Wang, H. Jing, F. Yan, H. R. Karimi, and N. Chen, "Optimization and finite-frequency H_∞ control of active suspensions in in-wheel motor driven electric ground vehicles," *J. Franklin Inst.*, vol. 352, no. 2, pp. 468–484, Feb. 2015, doi: 10.1016/j.jfranklin.2014.05.005.

[11] H. Pan, W. Sun, X. Jing, H. Gao, and J. Yao, "Adaptive tracking control for active suspension systems with non-ideal actuators," *J. Sound Vib.*, vol. 399, pp. 2–20, Jul. 2017, doi: 10.1016/j.jsv.2017.03.011.

[12] K. K. Afshar, A. Javadi, and M. R. Jahed-Motlagh, "Robust H_∞ control of an active suspension system with actuator time delay by predictor feedback," *IET Control Theory Appl.*, vol. 12, no. 7, pp. 1012–1023, May 2018, doi: 10.1049/iet-cta.2017.0970.

[13] T. Attia, K. G. Vamvoudakis, K. Kochersberger, J. Bird, and T. Furukawa, "Simultaneous dynamic system estimation and optimal control of vehicle active suspension," *Vehicle Syst. Dyn.*, vol. 57, no. 10, pp. 1467–1493, Oct. 2019, doi: 10.1080/00423114.2018.1521000.

[14] E. Enders, G. Burkhard, and N. Munzinger, "Analysis of the influence of suspension actuator limitations on ride comfort in passenger cars using model predictive control," *Actuators*, vol. 9, no. 3, p. 77, Aug. 2020, doi: 10.3390/act9030077.

[15] X. Zheng, H. Zhang, H. Yan, F. Yang, Z. Wang, and L. Vlacic, "Active full-vehicle suspension control via cloud-aided adaptive backstepping approach," *IEEE Trans. Cybern.*, vol. 50, no. 7, pp. 3113–3124, Jul. 2020, doi: 10.1109/TCYB.2019.2891960.

[16] J. J. Rath, M. Defoort, C. Sentouh, H. R. Karimi, and K. C. Veluvolu, "Output-constrained robust sliding mode based nonlinear active suspension control," *IEEE Trans. Ind. Electron.*, vol. 67, no. 12, pp. 10652–10662, Dec. 2020, doi: 10.1109/TIE.2020.2978693.

[17] Y. Zhang, Y. Liu, Z. Wang, R. Bai, and L. Liu, "Neural networks-based adaptive dynamic surface control for vehicle active suspension systems with time-varying displacement constraints," *Neurocomputing*, vol. 408, pp. 176–187, Sep. 2020, doi: 10.1016/j.neucom.2019.08.102.

[18] Z.-J. Fu and X.-Y. Dong, "H_∞ optimal control of vehicle active suspension systems in two time scales," *Automatika*, vol. 62, no. 2, pp. 284–292, Apr. 2021, doi: 10.1080/00051144.2021.1935610.

[19] M.-J. Hu, J. H. Park, and J. Cheng, "Robust fuzzy delayed sampled-data control for nonlinear active suspension systems with varying vehicle load and frequency-domain constraint," *Nonlinear Dyn.*, vol. 105, no. 3, pp. 2265–2281, Aug. 2021, doi: 10.1007/s11071-021-06690-y.

[20] L. Liu, C. Zhu, Y.-J. Liu, R. Wang, and S. Tong, "Performance improvement of active suspension constrained system via neural network identification," *IEEE Trans. Neural Netw. Learn. Syst.*, early access, Jan. 11, 2022, doi: 10.1109/TNNLS.2021.3137883.

[21] M. Park and S. Yim, "Design of static output feedback and structured controllers for active suspension with quarter-car model," *Energies*, vol. 14, no. 24, p. 8231, Dec. 2021, doi: 10.3390/en14248231.

[22] Y. Jeong, Y. Sohn, S. Chang, and S. Yim, "Design of static output feedback controllers for an active suspension system," *IEEE Access*, vol. 10, pp. 26948–26964, 2022, doi: 10.1109/ACCESS.2022.3157326.

[23] H. Jing, X. Li, and H. Karimi, "Output-feedback based H_∞ control for active suspension systems with control delay," *IEEE Trans. Ind. Electron.*, vol. 61, no. 1, pp. 436–446, Jan. 2014, doi: 10.1109/TIE.2013.2242418.
[24] D. E. Williams and W. M. Haddad, "Active suspension control to improve vehicle ride and handling," *Vehicle Syst. Dyn.*, vol. 28, no. 1, pp. 1–24, Jul. 1997, doi: 10.1080/00423119708969346.
[25] S. Ikenaga, F. L. Lewis, J. Campos, and L. Davis, "Active suspension control of ground vehicle based on a full-vehicle model," in *Proc. Amer. Control Conf. (ACC)*, Chicago, IL, USA, Jun. 2000, pp. 28–30, doi: 10.1109/ACC.2000.876977.
[26] M. Demić, I. Demić, M. Demić, and D. Diligenski, "A method of vehicle active suspension design," *Forschung Ingenieurwesen*, vol. 70, no. 3, pp. 145–158, Sep. 2006, doi: 10.1007/s10010-006-0025-5.
[27] F. Braghin, F. Resta, and E. Sabbioni, "A modal control for active/semi-active suspension systems," in *Proc. IEEE/ASME Int. Conf. Adv. Intell. Mechatronics*, Zurich, Switzerland, Sep. 2007, pp. 4–7, doi: 10.1109/AIM.2007.4412537.
[28] E. Katsuyama, "Decoupled 3D moment control for vehicle motion using in-wheel motors," *SAE Int. J. Passenger Cars-Mech. Syst.*, vol. 6, no. 1, pp. 137–146, Apr. 2013, doi: 10.4271/2013-01-0679.
[29] J. Yao, G. Lv, M. Qv, Z. Li, S. Ren, and S. Taheri, "Lateral stability control based on the roll moment distribution using a semiactive suspension," *Proc. Inst. Mech. Eng., D, J. Automobile Eng.*, vol. 231, no. 12, pp. 1627–1639, Oct. 2017, doi: 10.1177/0954407016681386.
[30] E. Enders, P. Karle, G. Bonelli, D. Killian, and G. Burkhard, "Modal vertical vehicle dynamics control for semi-active and active suspension systems," in *Proc. 15th Int. Conf. Ecol. Vehicles Renew. Energies (EVER)*, Monte-Carlo, Monaco, Sep. 2020, pp. 10–12, doi: 10.1109/EVER48776.2020.9242985.
[31] A. E. Bryson, Jr., and Y. Ho. *Applied Optimal Control*. New York, NY, USA: Taylor & Francis, 1975, p. 149.
[32] S. Yim, "Design of preview controllers for active roll stabilization," *J. Mech. Sci. Technol.*, vol. 32, no. 4, pp. 1805–1813, 2018, doi: 10.1007/s12206-018-0337-z.
[33] S. Sarpturk, Y. Istefanopulos, and O. Kaynak, "On the stability of discrete-time sliding mode control systems," *IEEE Trans. Autom. Control*, vol. AC-32, no. 10, pp. 930–932, Oct. 1987, doi: 10.1109/TAC.1987.1104468.
[34] V. L. Syrmos, C. T. Abdallah, P. Dorato, and K. Grigoriadis, "Static output feedback—A survey," *Automatica*, vol. 33, no. 2, pp. 125–137, 1997, doi: 10.1016/S0005-1098(96)00141-0.
[35] M. S. Sadabadi and D. Peaucelle, "From static output feedback to structured robust static output feedback: A survey," *Annu. Rev. Control*, vol. 42, pp. 11–26, Jan. 2016, doi: 10.1016/j.arcontrol.2016.09.014.
[36] G. Wang, C. Chen, and S. Yu, "Optimization and static output-feedback control for half-car active suspensions with constrained information," *J. Sound Vib.*, vol. 378, pp. 1–13, Sep. 2016, doi: 10.1016/j.jsv.2016.05.033.
[37] J. Mrazgua, R. Chaibi, E. H. Tissir, and M. Ouahi, "Static output feedback stabilization of T-S fuzzy active suspension systems," *J. Terramech.*, vol. 97, pp. 19–27, Oct. 2021, doi: 10.1016/j.jterra.2021.05.001.
[38] N. Hansen, S. D. Müller, and P. Koumoutsakos, "Reducing the time complexity of the derandomized evolution strategy with covariance matrix adaptation (CMA-ES)," *Evol. Comput.*, vol. 11, no. 1, pp. 1–18, Mar. 2003, doi: 10.1162/106365603321828970.
[39] J. K. Hedrick and T. Buetsen, "Invariant properties of automotive suspensions," *Proc. Inst. Mech. Eng., D, J. Automobile Eng.*, vol. 204, no. 1, pp. 21–27, 1990, doi: 10.1243/PIME_PROC_1990_204_128_02.
[40] D. Quaini, K. Sazgetdinov, V. Ivanov, and A. Ferrara, "Optimization based sliding mode control in active suspensions: Design and hardware-in-the-loop assessment," in *Proc. Eur. Control Conf. (ECC)*, Saint Petersburg, Russia, May 2020, pp. 1607–1612, doi: 10.23919/ECC51009.2020.9143835.
[41] G. Papaioannou, J. Jerrelind, and L. Drugge, "A study on skyhook-based suspension control algorithms with regards to tyre wear minimisation in hybrid vehicles," in *Proc. IEEE Int. Intell. Transp. Syst. Conf. (ITSC)*, Indianapolis, IN, USA, Sep. 2021, pp. 19–22, doi: 10.1109/ITSC48978.2021.9564409.
[42] D. Fényes, M. Fazekas, B. Németh, and P. Gáspár, "Implementation of a variable-geometry suspension-based steering control system," *Vehicle Syst. Dyn.*, vol. 60, no. 6, pp. 2018–2035, Jun. 2022, doi: 10.1080/00423114.2021.1890798.
[43] X. Hou, J. Zhang, Y. Ji, W. Liu, and C. He, "Autonomous drift controller for distributed drive electric vehicle with input coupling and uncertain disturbance," *ISA Trans.*, vol. 120, pp. 1–17, Jan. 2022, doi: 10.1016/j.isatra.2021.03.009.

MANBOK PARK received the B.S. degree in mechanical engineering from Inha University, South Korea, the M.S. degree in mechanical engineering from the Korea Advanced Institute of Science and Technology (KAIST), South Korea, in 2002, and the Ph.D. degree from the Graduate School of Convergence Science and Technology, Seoul National University, South Korea, in 2014.

He had been worked for 15 years at Mando Corporation, automotive part company. He is currently an Assistant Professor of electrical engineering at the Korea National University of Transportation. His research interests include autonomous vehicle, SLAM, precision map, risk assessment, and artificial intelligence.

YONGHWAN JEONG received the B.S. and Ph.D. degrees in mechanical engineering from Seoul National University, South Korea, in 2014 and 2020, respectively. From 2020 to 2021, he was a Senior Research Engineer with Hyundai Motor Company, South Korea. Since 2021, he has been an Assistant Professor with the Department of Mechanical and Automotive Engineering, Seoul National University of Science and Technology, South Korea. His research interests include sensor fusion with vehicular communication, risk assessment, driver intention inference with trajectory prediction, and motion planning and control of urban automated vehicle.

SEONGJIN YIM (Member, IEEE) received the B.S. degree in mechanical engineering from Yonsei University, South Korea, in 1995, and the M.S. and Ph.D. degrees in mechanical engineering from the Korea Advanced Institute of Science and Technology (KAIST), in 1997 and 2007, respectively.

From 2008 to 2010, he was a Postdoctoral Researcher with the BK21 School for Creative Engineering Design of Next Generation Mechanical and Aerospace Systems, Seoul National University. From 2011 to 2013, he was a Research Professor with the Advanced Institutes of Convergence Technology, Seoul National University. Since 2019, he has been an Associate Professor with the Department of Mechanical and Automotive Engineering, Seoul National University of Science and Technology, South Korea. His research interests include integrated chassis control systems with V2V communication, cloud computing-based vehicle control, electric power steering, and steer-by-wire systems.